Structural Properties of the Water/Membrane Interface of a Bilayer Built of the E. coli Lipid A

ARTICLE *in* THE JOURNAL OF PHYSICAL CHEMISTRY B · APRIL 2015

Impact Factor: 3.3 · DOI: 10.1021/jp5119629 · Source: PubMed

2 AUTHORS:

Krzysztof Murzyn
Jagiellonian University
24 PUBLICATIONS **705** CITATIONS
SEE PROFILE

Marta Pasenkiewicz-Gierula
Jagiellonian University
88 PUBLICATIONS **2,740** CITATIONS
SEE PROFILE

THE JOURNAL OF PHYSICAL CHEMISTRY B

Article

pubs.acs.org/JPCB

Structural Properties of the Water/Membrane Interface of a Bilayer Built of the *E. coli* Lipid A

Krzysztof Murzyn* and Marta Pasenkiewicz-Gierula

Department of Computational Biophysics and Bioinformatics, Faculty of Biochemistry, Biophysics, and Biotechnology, Jagiellonian University, Kraków, Poland

ABSTRACT: Lipid A is the most chemically invariant part of lipopolysaccharides (LPS). Both lipid A and LPS constitute the external layer of the outer membrane of Gram-negative bacteria. *E. coli*-specific hexacyl lipid A (ECLA) forms stable bilayers in the presence of sodium or magnesium cations. To characterize biologically relevant properties of the ECLA bilayer, and in particular its water/membrane interface, 800 ns molecular dynamics (MD) simulations of fully hydrated bilayers made of ECLA at 50 °C (i.e., 6 °C above the main phase transition) were performed. The validation of the computer model for the ECLA bilayer was performed using available experimental data. The overall good agreement with the data was found. An ECLA molecule makes on average ∼1.3 ion-mediated bridges with neighboring lipid molecules. The average number of interlipid hydrogen bonds is 2.7. The abundance of such intermolecular links results in tight packing of ECLA molecules in the bilayer and explains the relatively small value of the surface area per lipid (1.515 nm^2).

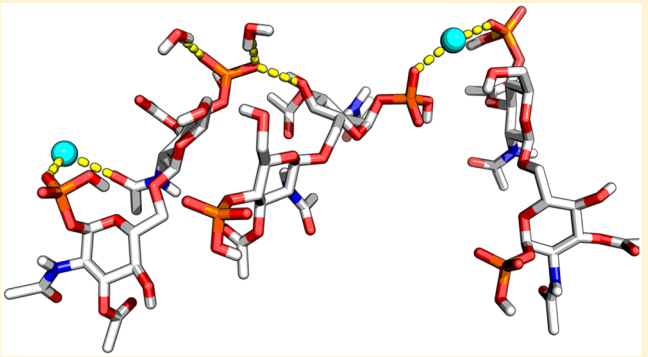

INTRODUCTION

The outer membrane of Gram-negative (G−) bacteria predominantly comprises lipopolysaccharide (LPS) and phosphatidylethanolamine in its outer and inner leaflet, respectively. LPS consists of a polysaccharide O-specific chain, an amphiphilic lipid A, and a core oligosaccharide region linking the two. Although lipid A is regarded as the most conserved part of LPS, it still exhibits considerable heterogeneity among different bacterial species and strains with structural variations involving both acyl chain length and distribution as well as substitutions of hydroxyl groups of the lipid A headgroup.

The hydrophilic part of a typical lipid A molecule (Figure 1) consists of α-D-glucosaminyl-(1 → 6)-β-D-glucosamine 1,4′-bisphosphate. At pH 7, two protonated phosphate groups in positions 1 and 4′ of proximal and distal pyranose rings, respectively, give a total charge of −2e on a single lipid A molecule. In wild type *E. coli* grown at 30 °C or above, the hydrophobic part of lipid A is made of (*R*)-3-hydroxymyristoyl chain [14:0(3-OH)] linked to glucosamine (GlcN) disaccharide in positions 2, 3, 2′, and 3′. The two $R\bar{3}$-hydroxy moieties of the distal GlcN are acylated with laurate and myristate, respectively, which are sometimes collectively referred to as the secondary hydrocarbon chains.

Lipid A and LPS are critical for maintaining integrity of the outer membrane of the Gram-negative bacteria. They also display a wide range of other biological activities. For example, LPS, which is released from lysed bacterial cells into the bloodstream during infection, initiates the acute inflammatory response known as sepsis or bacteremia, which, when not treated adequately,[1] can be life-threatening. Although it has been known for long that endotoxicity of LPS is embedded within lipid A,[2] which is recognized at picomolar levels by the TLR4/MD2 receptor complex of the innate immune system,[3,4] the molecular basis for processes triggered by lipid A or LPS remains largely uncharacterized.

One tentative hypothesis[5] emphasizes the need for characterization of the three-dimensional supramolecular assembly of lipid A molecules in the aqueous environment to elucidate its role in intercalation of bacterial lipids into eukaryotic cell membranes. This need cannot be easily satisfied due to thermotropic and lyotropic polymorphism of lipid A and LPS. What is more, the ability of lipid A to form various lamellar and nonlamellar phases depends on the presence and concentration of various biologically relevant cations and also on intrinsic structural properties of the lipid molecules. The unique feature of lipid A and LPS which renders the task very difficult is the fact that their chemical structure varies not only between different bacteria species but also during bacteria adaptation to ambient conditions. Moreover, the evolutionary or genetically gained ability of bacteria to modify the chemical structure of lipid A, and LPS is often related to increase in their disease-causing abilities (i.e., virulence), which makes studies on mechanisms that exploit these abilities especially important.

Due to the polymorphism of lipid A and the abundance of naturally occurring lipid A variants, it was uncertain for many

Received: December 1, 2014
Revised: March 12, 2015
Published: April 13, 2015

DOI: 10.1021/jp5119629
J. Phys. Chem. B 2015, 119, 5846−5856

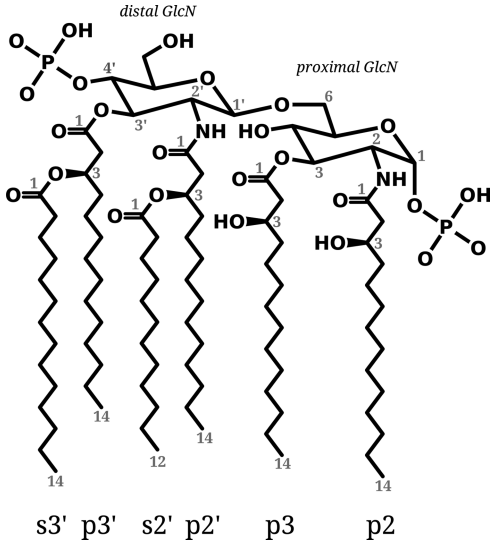

Figure 1. Chemical structure of *E. coli* lipid A (ECLA). Numbering of carbon atoms both in hydrocarbon chains and glucosamine (GlcN) disaccharide is in gray. Labeling of the ECLA acyl chains are in the bottom part of the figure (**p** and **s** letters stand for primary and secondary chains, respectively, and they are accompanied by numerical identifiers that indicate the position in GlcN disaccharide at which a particular acyl chain is attached).

years whether various kinds of lipid A form lamellar or nonlamellar structures under biologically relevant conditions, and in the case that lamellar phases are made, what is the main phase transition temperature. These questions were addressed by Naumann et al.,[6] who found that lipid A actually formed stable bilayer arrangements at 37 °C in the absence of divalent cations. However, under these conditions no stable closed vesicles were observed. The established temperature of the rather broad main phase transition (T_m) for synthetic lipid A 506 (LA-506), which corresponds to naturally occurring hexacyl bisphosphate *E. coli* lipid A (ECLA), was 44 °C.[6] Additionally, Naumann et al.[6] identified two other distinct phase transitions taking place at 27 and 38.5 °C and noted that even below T_m, considerable number of methylene segments of the acyl chains of lipid A assumed gauche conformations. The influence of divalent cations on lipid A phase behavior was studied by Seydel et al.,[7] who found that ECLA makes a lamellar phase at 20 °C with lipid A to Mg^{2+} molar ratio of 40:1. Between 37 and 55 °C, the lipid phase is mainly lamellar but with increasing temperature, coexistence of the inverted cubic phase is more and more pronounced. In preparations containing equimolar concentrations of ECLA and Mg^{2+}, the tendency toward forming inverted cubic phases increases, and coexistence of lamellar and inverted cubic phases is seen even at 20 °C.

In the vast majority of bacteria, lipid A is a part of LPS. However, in *F. tularensis*, 95% of lipid A molecules are not attached to LPS.[8] In the case of *E. coli*, it has been well-established that the minimal LPS required for these bacteria to sustain growth consists of lipid A with attached two 3-deoxy-α-D-*manno*-oct-2-ulosonic acid (α-Kdo) residues;[9] this compound is referred to as deep-rough LPS (dR-LPS). On the other hand, it is known that bacteria displaying a deep-rough phenotype are sensitive to detergents, hydrophobic antibiotics, and rough-specific bacteriophages. Colonies of such bacteria thrive only in a conducive environment. The growing size of the LPS headgroup in progression from lipid A through deep-rough LPS and rough LPS to smooth LPS is reflected in systematically lower values of T_m of relevant bilayers. For example, T_m for bilayers built of lipid A and dR-LPS with the same hydrocarbon chains[10] are ∼45 °C and ∼30 °C, respectively.

In the last 20 years, application of molecular dynamics (MD) simulation method to study lipid bilayers has provided valuable insight into understanding of molecular basis for their structural and dynamical properties. MD simulation studies of the model bacteria membranes made of lipid A or LPS are scarce. Recently, results of MD simulations of the outer membrane of *P. aeruginosa* containing rough LPS and dipalmitoylphosphatydylethanolamine (DPPE) at 25 °C have been reported.[11,12] Each of two simulations of the bilayer consisting of 64 LPS and 160 DPPE molecules covered 10 ns.[12] However informative, the simulations were too short to fully validate the employed AMBER95/GLYCAM93[13,14] force field parameters since they themselves did not converge to stable values of surface area per lipid. The slowly converging surface area for rough LPS and DPPE were approaching to, respectively, 1.08 and 0.43 nm^2, indicating that the model bilayer is in the gel phase. Such surface areas are consistent with expectations since T_m of the penta-acyl rough LPS bilayer is 30−37 °C[15] and that of the DPPE bilayer is 64 °C.[16]

Another attempt to model the outer bacterial membrane is reported by Piggot et al.[17] MD simulations of a bilayer built of Rd_1 chemotype of *E. coli* LPS, phosphatidylethanolamine, phosphatidylglycerol, and cardiolipin were carried out for 200 ns using the GROMOS 53A6 united-atom force field[18] extended recently by Kukol[19] to handle various kinds of lipid molecules. Even though some irregularities in mass density profiles and probability distributions of orientations of selected intramolecular vectors were clearly seen, the simulations were long enough to deepen our understanding of the molecular basis for electroporation of bacterial membranes.[17] Additionally, the study provided valuable estimates of structural parameters describing such lipid bilayers at Rd_1 LPS:Mg^{2+} molar ratio 1:5, including the surface area per lipid and the membrane width.

Recently Kirschner et al.[20] reported the extension of the GLYCAM force field to handle both phospholipids and LPS. The authors did not observe convergence in the surface area per lipid (SA) in a single 1 μs MD simulation of the asymmetric bacterial membrane with 72 penta-acyl rough LPS from *P. aeruginosa* in the upper leaflet and 180 dipalmitoylphosphatidylethanolamine (DPPE) molecules in the lower leaflet. Surpisingly, the MD simulations carried out at ∼27 °C and ∼77 °C gave the same surface area per LPS of ∼1.38 nm^2 and per DPPE of ∼0.55 nm^2.

Last year, a combined MD simulation/NMR spectroscopy study of *E. coli* LPS was reported.[21] MD simulations employed the CHARMM force field and were carried out at ∼37 °C for 300 ns. One of the model bilayers was built of 50 hexacyl lipid A molecules, which were in the deprotonated state resulting in the molecule net charge of −4e. Although the simulations were carried out 7 °C below T_m, the bilayer seemed to be in the liquid crystalline phase with SA of 1.68 nm^2. This value compares well with SA for the penta-acyl rough LPS at ∼77 °C reported by Kirschner et al.,[20] since in both cases, the surface area per lipid hydrocarbon chain is ∼0.28 nm^2. On the other hand, such a value exceeds ∼8% the upper limit of the sole experimental estimates of SA per LPS.[22]

DOI: 10.1021/jp5119629
J. Phys. Chem. B 2015, 119, 5846−5856

The aim of the present MD simulation study is to provide an atomic-detail view of a model lipid A bilayer at 50 °C, that is 6 °C above the main phase transition temperature. Such simulation conditions were chosen to enable comparison of the lipid A bilayer with appropriate results of experimental studies on reference bilayers built of either DPPC or lipid A/LPS. While most bacteria do not operate at such a high temperature, the conditions set in the simulations are biologically relevant, since many bacteria are occasionally exposed to increased temperature and employ versatile mechanisms of thermoadaptation such as, in particular, alteration of the acylation pattern of lipid A involving changes in distribution of lipid acyl chains, their number, length, and saturation. In our studies, we analyze configurations of a lipid A bilayer generated in two MD simulations employing the OPLS all-atom force field.[23] This force field has not been used previously to model lipid A or LPS-containing membranes. In the present study, we want to assess the stability of the lamellar phase made by hexacyl bisphosphate lipid A in the presence of sodium ions and to determine fundamental properties of such a bilayer on a submicrosecond timescale, focusing primarily on the structure of the water/membrane interface and interactions of lipid A with water and sodium ions. The structure of the lipid A molecule under study (ECLA, Figure 1) corresponds to lipid A occurring in the outer membrane of *E. coli*. The questions we address in the present paper are as follows: (1) is the lamellar arrangement of ECLA molecules stable on the multinanosecond time scale, (2) how the determined structural properties of the ECLA bilayer compare to available experimental data, (3) are there any preferred conformations of the $\beta 1 \rightarrow 6$ glycosidic linkage, (4) which ECLA atoms contribute most to various intermolecular interactions at the water/membrane interface. To provide answers to these questions, two 800 ns all-atom MD simulations of the fully hydrated ECLA bilayer were performed and thoroughly analyzed.

MATERIALS AND METHODS

Simulation Systems, Parameters, and Conditions. The simulation system was built of 72 *E. coli* lipid A (ECLA) molecules, 144 sodium ions, and 6192 water molecules, which sums up to 40248 atoms in total. A single ECLA molecule (Figure 1) consists of 299 atoms ($C_{94}H_{176}N_2O_{25}P_2$) and its molecular weight as a sodium salt, Na_2ECLA, is 1842.32 Da. ECLA molecules were arranged as a bilayer with 36 lipid molecules in each of the leaflets. The initial three-dimensional structure of the ECLA molecule was constructed in the PyMOL program[24] from small building blocks. A PDB file of the ECLA molecule was then processed by an in-house program, and the topology file was generated. OPLS all-atom (OPLS-AA) parameters,[25−27] supplemented with refined parameters for acyl chains and the phosphate group,[28] were assigned to ECLA molecules. Our modified force field parameters for the phosphate group[28] include van der Waals parameters for the oxygen atoms and partial charges, which were fitted to reproduce electrostatic potential determined in adequate electronic structure calculations for the model compound (i.e., dimethyl phosphate). The application of the new force field parameters assigned to the phosphate group were shown to lead to an improved reproduction of the enthalpy of vaporization of dimethyl phosphoric acid (i.e., the physical quantity which depends on the strength of intermolecular interactions). In our work,[28] we also reported a favorable reproduction of numerous condensed-phase properties of a long linear hydrocarbon chain (i.e., *n*-pentadecane) and improved description of interactions between water and the carboxyl group (as in methyl acetate). The refined OPLS-AA force field parameters have been successfully used in our recent MD simulations of a DPPC bilayer (to be published elsewhere), where experimentally available properties of this bilayer, including surface area per lipid, the membrane width, profiles of the deuterium order parameter, and absolute X-ray form factors, were correctly reproduced. In the comparison of different force fields for the study of disaccharides,[29] OPLS-AA was found to be a good alternative for GLYCAM, which was specifically developed to handle carbohydrates. In the case of two hydroxyphosphate groups present in the ECLA molecule (see Figure 1), either the original OPLS-AA parameters or the refined ones[28] were employed in comparative MD simulations (see below for further details). For water TIP3P model[30] and for sodium ions, Aqvist parameters[31] were used.

Construction, optimization, and MD simulation of the ECLA bilayers were carried out using Gromacs v4.5 package.[32] The initial configuration of the fully hydrated bilayer was constructed by arranging ECLA molecules manually and subjecting it to a series of short high-temperature and high-pressure MD simulation runs, which aimed at removal of both artificial ordering of ECLA molecules and superfluous voids in the membrane interior. The obtained pre-equilibrated ECLA bilayer was characterized by the surface area per lipid (SA) of 1.48 nm^2 and it was used as the initial system configuration (configuration **A**) in two subsequently performed MD simulations. The other initial configuration (**B**, SA = 1.70 nm^2) was generated in 50 ns MD simulation in which the temperature of ECLA molecules was elevated to 100 °C, and the temperature of water was kept at 37 °C. The employed MD simulation protocol preserved the ECLA bilayer structure but randomized conformations of individual ECLA molecules and their relative orientations. Two MD simulations which started from configuration **A** differed in OPLS-AA parameters assigned to ECLA hydroxyphosphate groups. In the first of the MD simulations, the original OPLS-AA parameters[25,26] were used while in the second one the refined parameters[28] were used. In the MD simulation, which started from configuration **B**, the refined OPLS-AA parameters were used.

The LINCS algorithm[33] was used to preserve the lengths of bonds involving hydrogen atoms in the ECLA molecules and the SETTLE algorithm[34] was used to constrain the water molecules. The time step was set at 2 fs. The Coulomb interactions were evaluated using the particle mesh Ewald summation.[35] In the real space, periodic boundary conditions with the usual minimum image convention were used in all three directions. A real-space cutoff of 1 nm, spline interpolation order of 6, and direct sum tolerance of 10^{-5} were used. The Lennard-Jones interactions were cut off at 1 nm. The list of nonbonded pairs was updated every 5 steps.

MD simulations were performed in the NPT ensemble under pressure of 1 atm and at a temperature of 323.15 K (50 °C) (i.e. 6 °C above T_m). The temperature of the solute (ECLA) and solvent (water and ions) were controlled independently. The temperature of the system was controlled by the Nose-Hoover method,[36,37] with the relaxation time constant of 0.5 ps. The pressure in the systems were controlled anisotropically by the Parrinello−Rahman method,[38] with the relaxation time constant of 5 ps. Calculations were done on the HP 2x220c cluster equipped in blade servers with dual Intel Quad Core

DOI: 10.1021/jp5119629
J. Phys. Chem. B 2015, 119, 5846−5856

Xeons E5450 interconnected with Infiniband 20 Gb/s at ~27 ns per day (64 CPU cores employed).

Simulation Analysis. The values of parameters describing properties of the ECLA bilayer were averaged over parts of trajectories, which were considered thermally equilibrated (see thermal equilibration of simulation systems in Results and Discussion).

Electron density profiles were calculated with an in-house program by counting selected atoms in consecutive slices of constant width (0.005 nm) along the bilayer normal.

In MD simulations of lipid bilayers, SA is reported as the average over all lipid molecules. With the membrane plane coinciding with the plane defined by two simulation box vectors, calculations of SA involve dividing the area of usually rectangular patch by the number of lipid molecules in one membrane leaflet. To get the distribution of SA determined for individual lipid molecules in the bilayer, one should compute a 2D Voronoi partition of the membrane plane. Each determined Voronoi cell, by definition, corresponds to the membrane region, which can be assigned univocally to a selected atom, group of atoms, or a molecule. The Voronoi cell in 2D adopts a shape of a polyhedra whose geometric center corresponds to a chosen point C_i assigned to a given group of n atoms projected on a plane. One unique property of a Voronoi cell is that its edges are equidistant to the two nearest sites: C_i and C_j. Computation of 2D Voronoi diagrams requires, in principle, a considerable amount of CPU time, and it is advisible to limit the number of points for which such a diagram is computed. A thorough discussion of various aspects of algorithms for computing Voronoi diagrams can be found in our paper[39] and references therein.

In this paper, a single molecular area[40] (SMA) (i.e., the area occupied by a lipid molecule in the bilayer) was calculated with an in-house program using the spatial module of the scipy Python package.[41] The calculations were done by constructing Voronoi tessellation for a set of ECLA atoms from a single bilayer leaflet. Periodic boundary conditions were handled by populating the analyzed set of atoms with their nearest neighbors' copies across the periodic boundaries (a default cutoff of 2 nm was used). Each acyl chain in the ECLA molecule was represented by a single point whose position corresponded to the position of the carbon atom no. 4 (Figure 1) projected on the bilayer plane. SMA was calculated as a sum of surface areas of relevant Voronoi polyhedra obtained for each of six acyl chains in a single ECLA molecule.

The conformation of the $\beta 1 \rightarrow 6$ glycosidic linkage in the ECLA molecule is expressed here in terms of ϕ (C6−O1′−C1′−O5′, c.f. Figure 1), ψ (C5−C6−O1′−C1′), and ω (O5−C5−C6−O1′) angles. Some alternative conventions in definition of these angles exist,[42] and one of the commonly used definitions of ϕ angle, ϕ_H, reads H1′−C1′−O1′−C6. The conversions between various conventions are straightforward;[42] however, violation of the ideal geometry for the sp3 anomeric carbon atom introduces small inaccuracies of up to 5°. For $\beta 1 \rightarrow 6$ linkage present in ECLA, the approximate formula for conversion between ϕ_H and ϕ reads: $\phi_H = \phi + 120°$.

The ECLA headgroup contains both glucosamine rings with the phosphate groups at positions 1 and 4′ and parts of acyl chains containing carboxyl, amide, ester, or hydroxyl groups (cf. Figure 1). With 27 hydrogen-bond (H-bond) acceptor atoms (eight of them are also H-bond donors), the ECLA headgroup offers many possibilities for making H bonds with water and lipid molecules. The presence of sodium ions adds another type of interaction of anionic ECLA molecules. In this paper, we employ geometric criteria for H-bond formation [i.e., distance between an H-bond donor (D) and acceptor (A) $\leq$ 0.325 nm and the angle ADH $\leq$ 30° (H is the hydrogen atom)]. Na^+ ions are considered to interact with ECLA molecules if the distance between Na^+ and an ECLA atom is $\leq$0.31 nm, which corresponds to the location of the first minimum in radial distribution function (RDF) determined for Na^+ and water oxygen atom (data not shown).

RESULTS AND DISCUSSION

Thermal Equilibration of Simulation Systems. To evaluate the process of thermal equilibration of the ECLA bilayer, the potential energy, E_{pot}, and SA were monitored during each of the MD simulations. SA was calculated from instantaneous box dimensions in the plane of the lipid bilayer.

The average values of E_{pot} and SA together with corresponding values of standard deviations, fluctuations, and total drifts are given separately for equilibration and production stages of the MD simulations in Table 1. The total drift in each case was determined by performing the least-square fit of data in a given period of time to a straight line and it is a product of the slope and the length of considered time range. The presence of a significant trend in the data manifests itself with the absolute value of total drift exceeding the standard deviation in the considered time range and also with the standard deviation visibly larger than fluctuations (i.e., root-mean-square deviations around the fitted trend line). As can be seen from Table 1, the first system with OPLS-AA refined parameters is well thermally equilibrated in both simulation stages owing to sufficiently long pre-equilibration runs performed during construction of its starting configuration (**A**). In case of the remaining simulation systems, large drifts in E_{pot} and SA are observed in the equlibration stage but not in the production stage (Table 1).

Table 1. Selected Control Parameters of MD Simulations Given per ECLA Molecule: Potential Energy (E_{pot}, in kJ/mol) and Surface Area (SA, in nm^2)[a]

	conf.	mean	stdev	fluctuations	total drift
		OPLS-AA Original Parameters			
E_{pot}	**A**	−5220	11	10	−13
		−5226	10	10	−2
SA	**A**	1.456	0.014	0.011	−0.028
		1.425	0.009	0.009	−0.001
		OPLS-AA Refined Parameters			
E_{pot}	**A**	−5087	10	10	−1
		−5086	10	10	0
SA	**A**	1.511	0.015	0.014	0.015
		1.515	0.013	0.013	0.008
E_{pot}	**B**	−5078	13	11	−23
		−5090	11	11	−2
SA	**B**	1.557	0.028	0.020	−0.066
		1.514	0.013	0.013	−0.009

[a]For both simulation stages (i.e. equilibration and production), the mean, standard deviation (stdev), fluctuations, and the total drift are given. In each case, the starting configuration (conf.) is shown in the row with statistics for the equilibration stage. The subsequent row contains statistics for the production stage.

The average values of E_{pot} and SA in systems employing the refined OPLS-AA parameters converged within 300 ns of their

DOI: 10.1021/jp5119629
J. Phys. Chem. B 2015, 119, 5846−5856

equilibration runs. Such a convergence is especially worth noting in the case of SA, as initially it drifted significantly (Figure 2). It should also be noted that the average values of

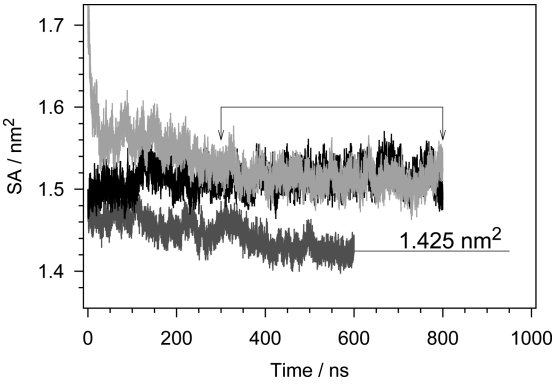

Figure 2. Time development of SA in the MD simulations using the refined OPLS-AA parameters (black and light gray) and the original OPLS-AA parameters (dark gray). Arrows indicate time span of the production runs of both MD simulations performed with refined OPLS-AA parameters. The other MD simulation was terminated at 600 ns with SA of 1.425 nm^2, indicating entering the model system into the gel phase.

both SA and E_{pot} are visibly lower when the simulation is performed with original OPLS-AA parameters. As the parameter set assigned to ECLA hydroxyphosphate groups is the only difference between two simulations starting from the same configuration (i.e., **A**), the observed difference in the average SA indicates that overestimated intermolecular interactions involving phosphate groups[28] can significantly influence structural properties of lipid bilayers.

To illustrate both convergence of SA in the simulations employing the refined OPLS-AA parameters and drift of SA in the reference simulation, time profiles of SA are shown in Figure 2. Since determination of structural parameters of a lipid bilayer requires that it is thermally equilibrated, in all subsequent analyses we use the last 500 ns fragments of trajectories generated in two simulations employing the refined OPLS-AA parameters. These parts of both trajectories are marked with arrows in Figure 2.

SA is notoriously difficult to obtain experimentally with high accuracy. This problem was discussed in great detail by Nagle and Tristram-Nagle[43] for dipalmitoylphosphatidylcholine (DPPC) bilayers, one of the most extensively studied model bilayers. The structural parameters describing the less frequently studied lipid A bilayers are relatively scarce. In X-ray diffraction studies[22] the upper limit of SA in the L_α ECLA bilayers is estimated as 1.56 nm^2. It corresponds well to the average SA in the ECLA bilayers obtained in this study of 1.5145 ± 0.0005 nm^2.

The visual inspection of the final configurations of the ECLA bilayer indicates (Figure 3) that it is in the L_α phase with no signs of collective ordering of the lipid acyl chains. The detailed analysis of the hydrocarbon core of the ECLA bilayer in the liquid crystalline phase will be published elsewhere.

Electron Density Profiles. The structure of a lipid bilayer is well-characterized by electron density profiles of chosen molecules or atomic groups. From density profiles (Figure 4), one can calculate the peak-to-peak and mean distances between various groups in opposing bilayer leaflets. The former distance is a measure of the bilayer thickness, while other cross-bilayer

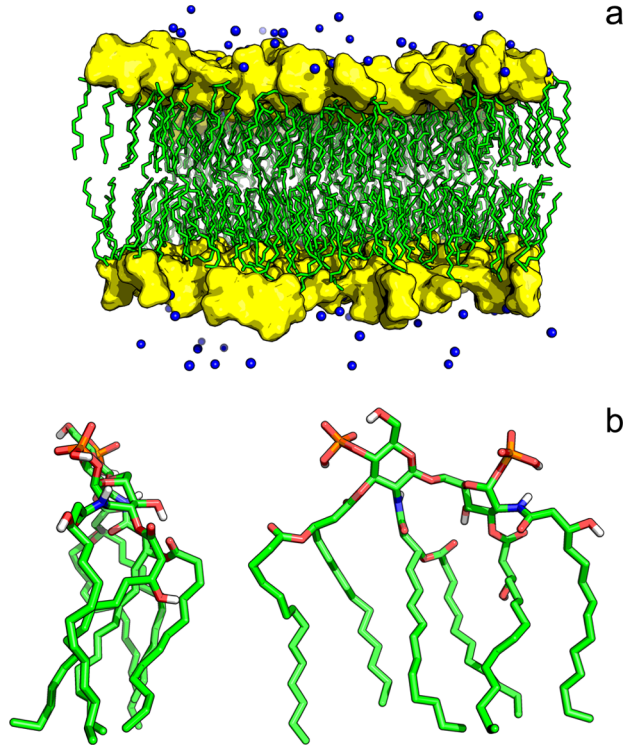

Figure 3. (a) A side view of a simulation box after 800 ns of MD simulation. ECLA headgroups are shown in yellow, hydrocarbon tails in green, and sodium ions in blue. Water molecules are omitted for clarity. (b) Two views of a single ECLA molecule randomly chosen from the configuration of the ECLA bilayer shown in (a).

distances are used to estimate dimensions of various bilayer regions, including the lipid/water interface and the hydrophobic core of the membrane.

The electron density profile for fully hydrated ECLA bilayer (Figure 4a) highlights the good convergence reached in the MD simulations. The largest differences between simulations are seen in the ~0.2 nm region of the water/membrane interface.

The average peak-to-peak distance determined from the relevant electron density profile in Figure 4a, D_{HH}, is 3.62 ± 0.01 nm. Among other definitions, one of the most commonly accepted is the Gibbs-Luzzati bilayer thickness,[43] D_B, which depends on the lipid molecular volume, V_L, and SA ($D_B = 2V_L/SA$). Recent calculations of V_L for the ECLA molecule performed with 3D Voronoi analysis toolkit[39] give V_L of 2.86 nm^3. As SA is 1.515 nm^2, D_B for the ECLA bilayer is estimated ~3.78 nm. Snyder et al.[22] performed X-ray diffraction analysis of bilayers built of various deep-rough LPS and rough LPS molecules in the gel and liquid-crystalline phases. Interestingly, the determined peak-to-peak distances in the gel phase (D_{HH} = 4.2 nm) were practically the same in the case of four studied chemotypes of LPS with peaks in electron density profiles corresponding to phosphate groups in lipid A. The same authors report also the width of a hydrocarbon region of the membranes in the gel phase (3.5 nm) at 22 °C and the liquid-crystalline phase (3.0 nm) at 50 °C. To estimate the width of the lipid A bilayer in the liquid-crystalline phase, we can follow the Snyder et al.[22] argument and assume that the transition from the gel to liquid-crystalline phase of a bilayer does not involve changing of the width of the bilayer interfacial region occupied by the lipid headgroups (i.e., steric headgroup

DOI: 10.1021/jp5119629
J. Phys. Chem. B 2015, 119, 5846−5856

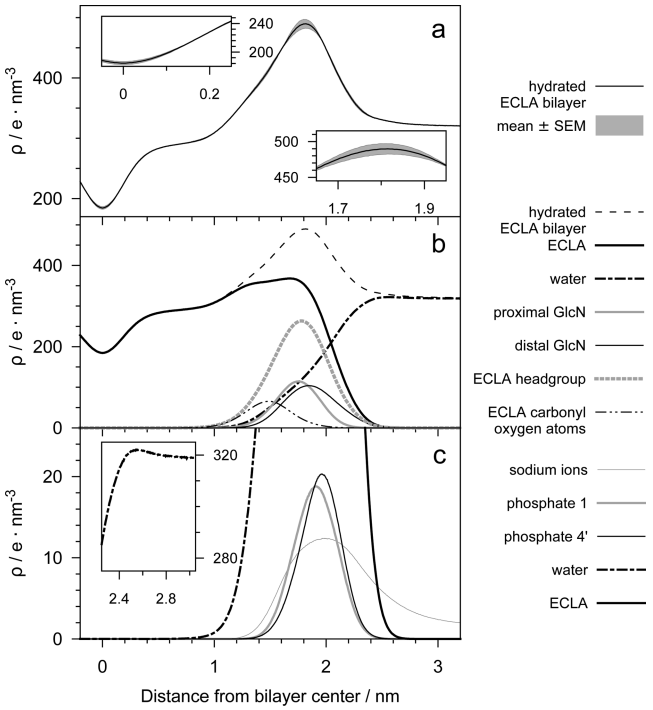

Figure 4. Electron density profile for the ECLA bilayer. (a) The total electron density determined for the hydrated ECLA bilayer [the average value is given together with corresponding standard error of the mean (SEM)]. Two selected regions of the profile are shown in the insets. (b and c) The average electron density profile for various molecular parts of the hydrated ECLA bilayer (see legend on the right). The inset in (c) shows increased electron density of water at the outer boundary of the water/ECLA membrane interface.

thickness[43]). In other words, the change of the membrane width observed in such a transition can be assigned exclusively to thinning of the hydrocarbon core of the bilayer. Such an assumption is not unreasonable since no change in steric headgroup thickness was observed for bilayers built of phosphotidylethanolamine or phosphotidylcholine.[43] With the above assumption, the width of the lipid A bilayer in the liquid-crystalline phase is ~3.7 nm. This value agrees well with 3.62 nm determined in the reported MD simulations. Interestingly, the determined width of the ECLA membrane compares surprisingly well with D_{HH} of 3.84 nm obtained for DPPC bilayer[44] at 50 °C, given minor differences in the structure of the hydrocarbon chains of both lipids and a major dissimilarity of their headgroups.

As can be seen in Figure 4b, the electron density distributions for both GlcN rings are slightly shifted into the bilayer interior as compared to the positions of both ECLA phosphate groups (Figure 4c). Thus, the structure of ECLA in Figure 1, although chemically correct (cf. 1-phosphate group in the α-anomeric position of the proximal glucosamine) is somewhat misleading since, as shown in Figure 4c, 1-phosphate group is actually pointed into the water phase due to the available conformations of the glycosidic linkage between two GlcN rings. What is more, the relative position of 1-phosphate and 4′-phosphate groups indicate that the ECLA headgroup is slightly tilted with respect to the plane of the membrane with the 1-phosphate group closer to and 4′-phosphate group further from the membrane center. The above interpretation of the electron density profiles is supported by trans membrane peak-to-peak distances calculated for corresponding atomic groups, which are 3.51 nm (the proximal GlcN), 3.69 nm (the distal GlcN), 3.82 nm (1-phosphate), and 3.92 nm (4′-phosphate). SEM values in all cases are 0.02 nm or less. The inward tail of the electron density distribution of the proximal GlcN ring is well-aligned with water density profile which decrease in this region of the membrane/water interface. While the maxima of the distributions of both GlcN rings are close to each other, the distribution of the distal GlcN ring is visibly broader, indicating both higher mobility of that part of the ECLA molecule and its larger exposition to the water phase.

Maxima of the distributions of the sodium ions and 1- and 4′-phosphate groups are also close to each other (Figure 4c), indicating preferable interactions between the cations and the bulky anionic groups. Density profile of sodium ions approach zero ~0.2 nm closer to the membrane center than is the case of both phosphate groups. The long tail of the sodium ions distribution extends into the water phase, which indicates that a significant number of cations is not bound to ECLA (c.f. Figure 3). Since the system contains the number of sodium ions exactly compensating the overall charge of the ECLA molecules, the presence of freely diffusing sodium ions in the intervening water indicates that the surface of ECLA bilayer remains slightly anionic. It is also interesting to note that the water density profile has flat maxima in direct proximity of the bilayer surface (inset in Figure 4c). The electron density increases in that region from 318.5 e/nm^3 up to 322 e/nm^3 at 2.56 nm from the bilayer center. Such a change in the water density stems from increased ordering of water molecules in that region of the water/membrane interface.[45]

Single Molecular Area. Single molecular area (SMA) is the area occupied by a lipid molecule in the bilayer.[40] In Figure 5, distributions of SMA are shown separately for both replica

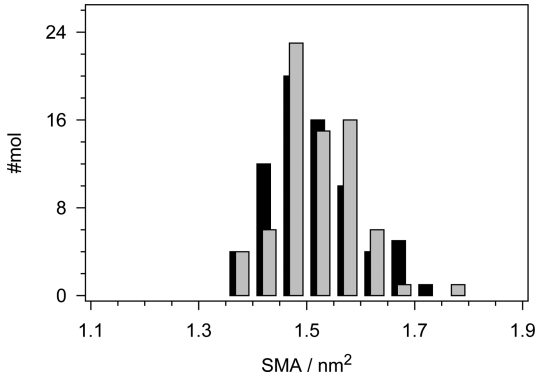

Figure 5. Distributions of time-averaged SMA for ECLA molecules in two replica simulation systems.

simulation systems. For each ECLA molecule, the time average SMA was computed and tabulated in the histogram with bin size of 0.05 nm^2. The ensemble averages (standard deviations) of SMA are 1.515 ± 0.073 nm^2 and 1.514 ± 0.081 nm^2 for two replica MD simulations. To evaluate statistical significance of differences between these two distributions of SMA, we used the Kolmogorov−Smirnov test. The p value of 0.87 indicates that these distributions are statistically indifferent. The observed convergence in distributions of SMA is worth emphasizing since the initial ones were well-separated with markedly different average SAs (c.f. Figure 2). It also confirms that both simulation systems are thermally well-equilibrated. Another feature of these distributions worth noting is the

DOI: 10.1021/jp5119629
J. Phys. Chem. B 2015, 119, 5846−5856

presence of small fractions of ECLA molecules with SMA lower than 1.40 nm^2 (on average ~6% of ECLA molecules have such SMAs), and an even smaller number have SMA higher than 1.70 nm^2 (~1%).

Conformation of ECLA Glycosidic Linkage. Probability distributions of ϕ, ψ, and ω angles (see Materials and Methods for details) are shown in Figure 6. These dihedral angles

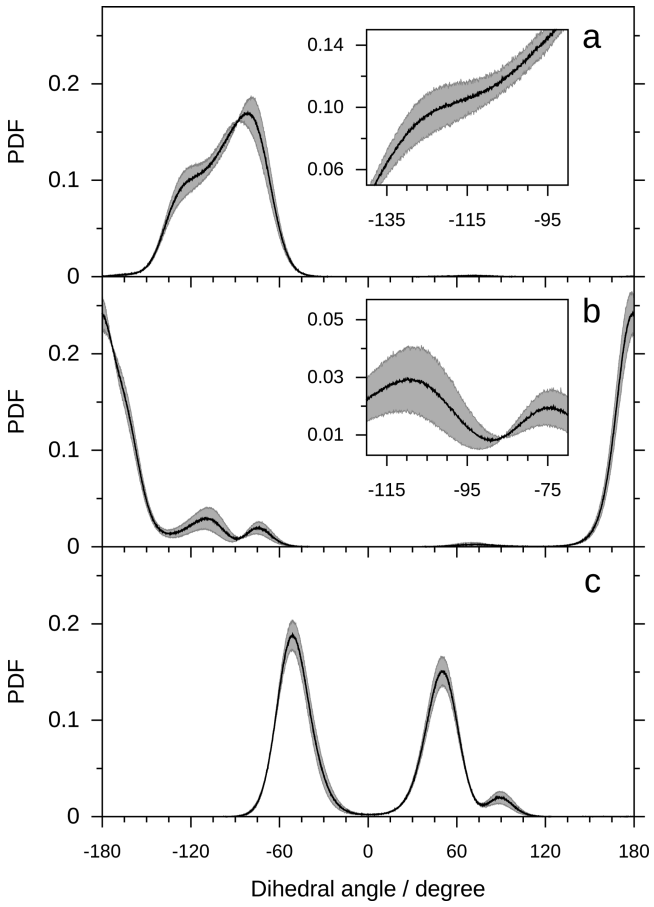

Figure 6. Probability distributions (PDFs) of ECLA (a) ϕ, (b) ψ, and (c) ω angles in ECLA. The inset in (a) shows a region close to the inflection point between maxima preliminarily assigned to two subpopulations of ϕ angle conformers (see the main text for details). The inset in (b) shows a region of ψ angle distribution corresponding to its two minor subpopulations which differ in relative occurrence in two replica simulation systems.

determine relative orientations of two GlcN rings and, in practice, allowed conformations of the ECLA headgroup. Differences between two replica simulations are relatively small and generally in the values of maxima of appropriate probability density functions (PDFs) (i.e., relative occurrence of the most probable conformations).

The distribution of ϕ angles shows a broad peak, ranging from −150° to −45° with a well-resolved local maximum at −82°. The shape of the distribution indicates the presence of at least two subpopulations of conformers with overlapping ϕ angles distributions. To provide qualitative interpretation of the observed ϕ angle distribution, one can assume that fluctuations of the angle in each subpopulation can be described by a normal distribution and use expectation maximization to determine parameters of such a mixture of gaussians. Each subpopulation of conformers identified in that way is described by the average value of a dihedral angle and corresponding standard deviation. The decomposition of the dihedral angle profiles into a mixture of gaussians was performed with the PyMix Python module.[46] For the ϕ angle distribution, two major contributions from subpopulations with −82° ± 14° (relative occurrence 58%) and −118° ± 16° (42%) were found. The distribution of ψ angles shows three well-resolved peaks. The analysis of this mixture of gaussians leads to resolution of three distinct subpopulations of ψ angle conformers with −177° ± 17° (87%), −111° ± 12° (9%), and −74° ± 8° (4%). Finally, in the average distribution of the ω angle, there are three well-resolved peaks. They can be assigned to the following subpopulations of ω angle conformers: −49° ± 12° (53%), 49° ± 12° (43%), and 91° ± 8° (4%).

The determined conformational preferences of the glycosidic linkage of the ECLA headgroup are compared with those in crystal structures of reference compounds from the Cambridge structural database (CSD) and research collaboratory for structural bioinformatics protein data bank (RCSB PDB) in Table 2. In CSD, two entries with disaccharides sharing the

Table 2. Conformations of β1 → 6 Glycosidic Linkage as Emerging from Selected Crystal Structures[a]

molecule name	ϕ (deg)		ψ (deg)		ω (deg)	
gentiobiose	−58		−156		−62	
macrozamin	−78		−104		66	
eritoran	−74		−170		−84	
R-LPS	−64		−131		−66	
ECLA	-82_{14}	58%	-177_{17}	87%	-49_{12}	53%
	-118_{16}	42%	-111_{12}	9%	49_{12}	43%
			-74_{8}	4%	91_{8}	4%

[a]Subpopulations of ϕ, ψ, and ω ECLA conformers are identified by the average value of a dihedral angle and the corresponding standard deviation (in subscript). The percentage occurrences of the conformers are also given. See the main text for details.

glycosidic linkage type with ECLA were found: gentiobiose (6-*O*-β-D-glucopyranosyl-D-glucose, entry GENTBS[47]) and macrozamin (a derivative of primeverose (6-*O*-β-D-xylopyranosyl-D-glucose), MCRZMA[48]). To identify crystal structures of ECLA headgroup analogues deposited in the RCSB PDB, the SMILES query C1CCC[C@@H](O1)OCC2CCCCO2 encoding β1 → 6 linked pyranoses was run. The SMILES expression was produced with PubChem Sketcher.[49] In the RCSB PDB search results, structures of two different ligands were particularly informative: eritoran, an investigational drug showing a remarkable resemblance to a tetracyl lipid A (RCSB PDB entry 2Z65[50]) and a rough LPS (R-LPS) molecule (1FI1[51]) from *E. coli*.

As can be seen in Table 2, there is a spread of possible conformations of β1 → 6 linkage among crystal structures of chemically different molecules sharing the same configuration of two hexopyranoses. Such a spread is also observed in values of ϕ, ψ, and ω angles determined here for ECLA. Thus, conformations of the ECLA glycosidic linkage fit well to the experimental data. In the case of the ϕ angle, the conformations frequently populated in MD simulations with the average value of −118° is actually not observed in the crystal structures. On the other hand, two major subpopulations of the ψ angle conformers are both seen in the crystal structures. Finally, let us note that the least frequently populated conformations of the angles ψ and ω (i.e., −74° and 91°, respectively) are not

DOI: 10.1021/jp5119629
J. Phys. Chem. B 2015, 119, 5846−5856

observed in crystal structures; however, at this point, it is difficult to say if this is a consequence of deficiencies in the parametrization of certain angle types in OPLS-AA or the experimental data is too scarce to display such conformations.

Correlation between the Glycosidic Linkage Conformation and the ECLA Single Molecular Area. Possible correlations between determined above conformations of ϕ, ψ, and ω angles of the glycosidic linkage of ECLA (c.f. Figure 6 and Table 2) and single molecular areas occupied by individual ECLA molecules (SMA) were investigated. For distinguished states of ϕ, ψ, and ω torsion angles, one-letter symbols were assigned which were subsequently used in denoting individual conformers of ECLA. Since some conformations of the dihedral angles were characterized by heavily overlapping distributions (c.f. Table 2), an unambiguous assignment of the state symbols was not always possible. Consequently, based on the distributions in Figure 6, the following definitions of the dihedral conformers were used. For the ϕ angle, only one conformer (A) was defined with ϕ between $-160°$ and $-30°$ ($-160° < \phi < -30°$). For the ψ angle, three conformers were defined: (M) with $-135° < \psi < -40°$; (N) with $45° < \psi < 105°$; and (O) with $\psi < -140°$ or $\psi > 120°$. Finally, for the ω angle, two conformers were defined: (R) with $-90° < \omega < -10°$ and (S) with $10° < \omega < 115°$. Thus, for example, AOR denotes the ECLA conformation with ϕ, ψ, and ω angles in states A, O, and R, respectively. Such conformer tags were assigned for all consecutive configurations of individual ECLA molecules and stored in the form of conformer trajectories together with independently calculated instantaneous values of SMA. Then, for each nonoverlapping 100 ps chunks (i.e., for 50 consecutive conformations) of the conformer trajectories characterized by a single conformational sequence of the dihedral states, the average SMA value was recorded. The relative occurrence of various conformers and the corresponding SMA values are collected in Table 3. This analysis was performed for both replica MD trajectories, and the reported results are arithmetic averages with corresponding standard errors (in subscript).

Table 3. Relative Occurrence of ECLA Diglucosamine Conformers Together with Corresponding SMA Values[a]

ctag	occurrence (%)	SMA (nm^2)
AOS	$34.7_{4.3}$	$1.503_{0.002}$
AOR	$39.1_{0.3}$	$1.526_{0.001}$
AMS	$4.2_{1.4}$	$1.561_{0.061}$
AMR	$5.6_{2.4}$	$1.452_{0.043}$

[a]For explanation of conformer symbols (ctag), see the main text.

As can be seen from Table 3, four major conformers of the glycosidic linkage can be identified for over 83% of the ECLA conformations. Conformations comprising the N state of the ψ angle are found in less than 1% of all identified ECLA conformations. The remaining 16% are either short-lived (i.e., <100 ps) or comprise unassigned dihedral states of ϕ, ψ, and ω angles. For two pairs of the conformers with the same conformations of ϕ and ψ angles (i.e., AOS/AOR and AMS/AMR), the difference in their occurrence is statistically insignificant. On the other hand, the average SMA values assigned to various ECLA conformers are different at a significance level of 0.05 (cf. AOS/AOR, AMS/AMR, and AMR/AOR). It should be noted here that SMA values might be used to describe compactness of an ECLA molecule in the bilayer. ECLA molecules with the glycosidic linkage in the AMR conformation are the most compact while those with the AMS conformation are the most relaxed. The differences in compactness of ECLA are less pronounced for the two most common conformers (i.e., AOS and AOR). While data in Figure 5 may suggest somewhat static picture of the SMA distribution, it should be noted that SMA changes rapidly in time (data not shown), which reflects dependence of this structural parameter on the collective dynamics of spatially close lipid molecules.

The analyses of the conformer trajectories allowed us also to assess the sampling of conformational space accessible to the glycosidic linkage of individual ECLA molecules. Each ECLA molecule, during the 0.5 μs-MD simulation, adopted on average 3.54 ± 0.03 distinct conformations, and the majority of ECLA molecules visited many times all four major conformations of the glycosidic linkage.

Interactions of ECLA with Water and Sodium Ions. The ECLA headgroup with 27 H-bond acceptor/donor atoms makes on average 17.9 H bonds with water molecules. H bonds made between two atoms of the same ECLA molecule (the intramolecular H bonds) are less frequent than H bonds made between atoms of two neighboring ECLA molecules (the intermolecular H bonds). There are 0.99 ± 0.27 intramolecular and 2.70 ± 0.33 intermolecular H bonds per single ECLA molecule (Table 4).

Cations counterbalancing the negative net charge of ECLA molecules bind to the oxygen atoms of the ECLA headgroup. On average, each headgroup binds 1.13 ± 0.08 sodium ions (Table 4), and the majority of ions are simultaneously bound by more than one oxygen atom, forming either intramolecular or intermolecular ion bridges. There are 0.84 ± 0.07 intramolecular and 1.27 ± 0.14 intermolecular ion bridges per ECLA (Table 4). Ion bridging has been described in the literature before, however, only in the case of phosphatidylcho-

Table 4. Statistics of Interactions between ECLA, Water, and Sodium Ions[a]

	Op	Oc	OHg	OHt	Oe	Ope	Oce	N	Σ
H bonds with water	9.09_{6}	2.83_{8}	2.53_{2}	1.29_{2}	1.17_{2}	0.29_{1}	0.04_{1}	0.66_{2}	17.89_{24}
intramolecular H bonds	0.34_{1}	0.18_{1}	0.35_{1}	0.0	0.05_{1}	0.0	0.0	0.04_{2}	0.99_{27}
intermolecular H bonds	0.74_{3}	0.59_{3}	0.28_{2}	0.72_{2}	0.01_{1}	0.02_{1}	0.0	0.33_{1}	2.70_{38}
bound Na^+ ions	0.70_{2}	0.20_{3}	0.11_{1}	0.05_{1}	0.07_{1}	0.01_{1}	0.0	0.0	1.13_{8}
intramolecular ion bridges	0.42_{1}	0.16_{3}	0.04_{1}	0.0	0.21_{1}	0.02_{1}	0.0	0.0	0.84_{7}
intermolecular ion bridges	0.77_{5}	0.26_{5}	0.07_{1}	0.10_{1}	0.06_{1}	0.01_{1}	0.0	0.0	1.27_{14}

[a]Average numbers of H bonds made between ECLA and water molecules; intra- and intermolecular ECLA H bonds; Na^+ ions bound to ECLA atoms; and intra- and intermolecular ion bridges are shown together with corresponding standard errors (SEM, in subscript as hundredth parts). Labeling of atom groups is described in the main text.

DOI: 10.1021/jp5119629
J. Phys. Chem. B 2015, 119, 5846−5856

line (PC) and phosphatidylserine (PS) bilayers.[52−54] The representative 3D structures illustrating relevant intra- and intermolecular lipid A interactions, as well as interactions with cations, are shown in Figure 7.

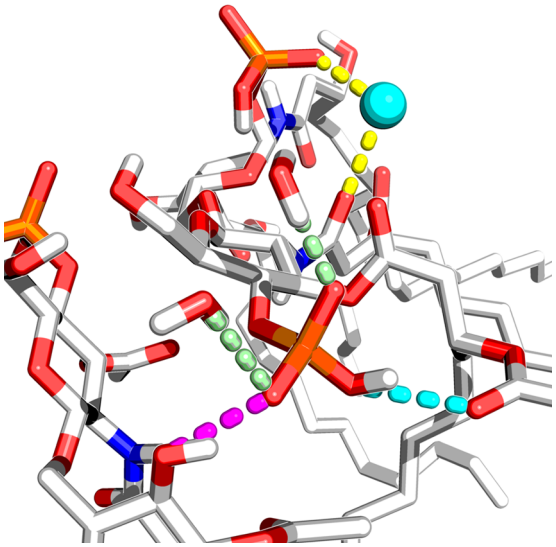

Figure 7. Intermolecular interactions in the water/membrane interface of the ECLA bilayer. H bonds between water and the 4′-phosphate group of ECLA are shown in pale green, intra- and interlipid H-bond are shown in cyan and pink, respectively, and a single intralipid ion bridge is shown in yellow.

As can be seen from data collected in Table 4, various polar groups, which are present in the ECLA headgroup, contribute differently to interactions occurring at the bilayer/water interface.

The largest contribution to all intermolecular interactions have six oxygen atoms of the phosphate groups (Op, Figure 1), which make 51% of all H bonds with water molecules and bind over 62% of Na^+ in contact with all ECLA atoms. The second largest group constitute six carbonyl oxygen atoms (Oc, Figure 1), which make 16% of all H bonds with water molecules and bind 18% of Na^+ ions and two oxygen atoms in GlcN hydroxyl groups (OHg) which make 14% H bonds with water and bind ∼10% Na^+ ions. Interactions with water and Na^+ ions involving hydroxyl groups of acyl chains (OHt: 7%/4% water/Na^+) and three ether oxygen atoms (Oe: 7%/6% water/Na^+) are less frequent. Both kinds of ester oxygen atoms (i.e., carboxylate, Oce, and phosphate, Ope, ester atoms) do not bind Na^+ ions. Additionally, Oce practically do not interact with water, while Ope occasionally bind water molecules, but such interactions are relatively rare (on average, one water molecule per six Ope atoms). Finally, nitrogen atoms at positions 2 and 2′ (N) do not contribute much to interactions between ECLA and water as they bind, on average, one water molecule per three nitrogen atoms. Furthermore, no contacts between N atoms and Na^+ ions are made.

Intramolecular H bonds involve predominantly (∼88%) Op, OHg, and Oc. Interestingly, OHt and N practically do not participate in intramolecular H bonds but contribute significantly (∼44%) to intermolecular H bonds.

When compared to PC in fully hydrated bilayers in the L_α phase in terms of Na^+ binding, ECLA binds Na^+ predominantly by Op atoms (Table 4), whereas PC by Oc atoms but also Op atoms.[52−54] This difference can be attributed to shielding of the Oc atoms in the ECLA from Na^+ by the bulky pyranose rings, a much greater number of the Op atoms, of six, than that of the Op atoms of the PC headgroup, of two and also low hydration of the Oc atoms (Figure 4b).[54] Also, Op atoms participate by far more than other oxygen atoms in formation of intermolecular ion bridges (∼61% of all ion-bridges); the second most involved are Oc atoms (∼20% of all ion-bridges). Distribution of the binding multiplicity of Na^+ ions interacting with ECLA oxygen atoms is shown in Figure 8. As can be seen,

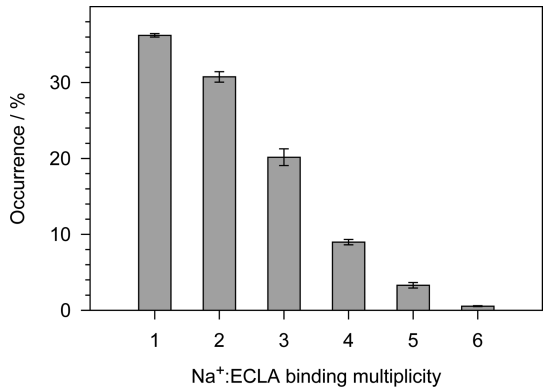

Figure 8. Distribution of the binding multiplicity of Na^+ ions interacting with ECLA oxygen atoms. The average percentage occurrence of binding multiplicities are shown together with corresponding standard errors.

36.2% ± 0.2% of ECLA-bound Na^+ ions make just one contact with ECLA oxygen atoms. The remaining Na^+ ions make up to 6 contacts [i.e., they form either intra- or intermolecular ion bridges (cf. Table 4)].

CONCLUSIONS

Three computer models of the fully hydrated *E. coli* lipid A (ECLA) bilayer in the presence of Na^+ ions were generated with MD simulations at 323.15 K (50 °C), that is 6 K above T_m of 317.15 K (44 °C). Two of them had the same modified OPLS-AA parameters[28] assigned to ECLA molecules but different initial configurations of molecules and distributions of velocities and were MD simulated for 800 ns. ECLA molecules in the third simulation system were parametrized with the modified OPLS-AA parameters[28] assigned to acyl chains and the original OPLS-AA parameters[25,26] assigned to the remaining ECLA atoms. The MD simulation of the third system was carried out for 600 ns. The first two systems were in the proper L_α phase, whereas the third system was entering an improper gel phase; thus, it was neither simulated further nor analyzed.

Thermal equilibration of the bilayers was long as systems reached equilibrium in ∼300 ns of MD simulations.

The bilayers were validated against scarce experimental data, including surface area per lipid, the membrane width, and known conformations of the $\beta 1 \rightarrow 6$ glycosidic linkage in carbohydrates, showing structural similarity to the diglucosamine part of lipid A.

The average surface area per ECLA (SA) as well as a surface area of each ECLA molecule (single molecular area, SMA) were calculated. The latter ones were calculated using 2D Voronoi tessellation method. The average SA is 1.514 nm^2. SMA values span a relatively large range from 1.36 to 1.76 nm^2.

DOI: 10.1021/jp5119629
J. Phys. Chem. B 2015, 119, 5846−5856

A detailed analysis of conformers of the glycosidic linkage was performed, and four major subpopulations were identified and compared with relevant crystallographic data. The determined conformers agree well with experimental data.

The number of intermolecular H bonds and ionic bridges at the water/ECLA bilayer interface has been determined for the first time. An ECLA headgroup makes, on average, 17.9 H bonds with water molecules and 2.7 H bonds with other ECLA headgroups. Additionally, it binds, on average, 1.13 Na^+ ions, mainly via Op atoms. Sodium ions are mostly bound by more than one ECLA oxygen atom, and they make 1.27 intermolecular ion bridges per ECLA.

The electron density profile for water molecules indicates that they do not extend further than ECLA phosphate oxygen atoms and barely reach carbonyl oxygen atoms. Thus, the water penetration of the ECLA bilayer is lower than that of PC bilayers.

Numerous intermolecular interactions at the bilayer/water interface of the ECLA bilayer are the reason for the relatively small SA. This results in a tight packing of lipid molecules in the bilayer, which, together with a large number of polar groups of the ECLA headgroup, make the bilayer less permeable to water, ions, and small polar compounds. As the ECLA bilayer is a simplified model of the outer bacteria membrane, one can expect that the membrane constitute a high permeability barrier.

The present study of the bilayer built of lipid A molecules containing six fully saturated acyl chains provides a useful reference system for future research regarding the effect of the acylation pattern of lipid A on the properties of model membranes built of LPS and its role in thermoadaptation of the bacteria. The experience gained in the presented study can be useful in building a more complex bilayer consisting of LPS, of which lipid A is an integral part. This study revealed strong interlipid links and numerous H bonds with water in the interfacial region of the ECLA bilayer. One can expect that these interactions reduce water penetration across the lipid matrix of the bacterial outer membrane. At the interface, also sodium ions are readily bound to the polar groups of ECLA, which most likely hinders their passive diffusion across the matrix. Altogether, the lipid A bilayer emerges as a solid barrier, which provides a bacterial cell with reliable protection against hazardous environmental factors. These protective features of the lipid A bilayer can only be strengthened by the presence of densely packed long polysaccharide chains of LPS in the outer bacterial membranes.

AUTHOR INFORMATION

Corresponding Author

*E-mail: krzysztof.murzyn@uj.edu.pl.

Author Contributions

K.M. conceived the study, constructed computer models of lipid bilayers, carried out MD simulations, designed and implemented required software tools for analysis of MD trajectories, performed MD simulation analyses, and wrote the manuscript with scientific input from M.P.-G. M.P.-G. performed a critical reading of the manuscript and deepened discussion on ion bridges by referring to literature data concerning phospholipid bilayers. Both authors read and approved the final version of the manuscript.

Notes

The authors declare no competing financial interest.

ACKNOWLEDGMENTS

This work is supported by the Polish National Science Center under Grant 2011/01/B/NZ1/00081 and in part by Polish Ministry of Science and Information Technology under Grant PBZ-MNiI-1/1/2005. Faculty of Biochemistry, Biophysics and Biotechnology is a partner of the Leading National Research Center (KNOW) supported by the Ministry of Science and Higher Education.

REFERENCES

(1) Yin, N.; Marshall, R.; Matheson, S.; Savage, P. Synthesis of Lipid A Derivatives and Their Interactions with Polymyxin B and Polymyxin B Nonapeptide. *J. Am. Chem. Soc.* **2003**, *125*, 2426−2435.

(2) Rietschel, E. T.; Galanos, C.; Tanaka, A.; Ruschmann, E.; Luderitz, O.; Westphal, O. Biological Activities of Chemically Modified Endotoxins. *Eur. J. Biochem.* **1971**, *22*, 218−224.

(3) Dinarello, C. A. Interleukin-1 and Interleukin-1 Antagonism. *Blood* **1991**, *77*, 1627−1652.

(4) Resman, N.; Vasl, J.; Oblak, A.; Pristovsek, P.; Gioannini, T. L.; Weiss, J. P.; Jerala, R. Essential Roles of Hydrophobic Residues in Both MD-2 and Toll-like Receptor 4 in Activation by Endotoxin. *J. Biol. Chem.* **2009**, *284*, 15052−15060.

(5) Brandenburg, K., Seydel, U. In *Lipid A in Cancer Therapy*; Jeanin, J.-F., Ed.; Advances in Experimental Medicine and Biology; Landes Bioscience and Springer Science+Business Media: New York, 2010; Vol. *667*.

(6) Naumann, D.; Schultz, C.; Born, J.; Labischinski, H.; Brandenburg, K.; von Busse, G.; Brade, H.; Seydel, U. Investigations into the Polymorphism of Lipid A from Lipopolysaccharides of *Escherichia Coli and Salmonella Minnesota* by Fourier-Transform Infrared Spectroscopy. *Eur. J. Biochem.* **1987**, *164*, 159−169.

(7) Seydel, U.; Brandenburg, K.; Koch, M. H. J.; Rietschel, E. T. Supramolecular Structure of Lipopolysaccharide and Free Lipid A Under Physiological Conditions As Determined by Synchrotron Small-Angle X-Ray Diffraction. *Eur. J. Biochem.* **1989**, *186*, 325−332.

(8) Wang, X.; Ribeiro, A. A.; Guan, Z.; McGrath, S. C.; Cotter, R. J.; Raetz, C. R. H. Structure and Biosynthesis of Free Lipid A Molecules That Replace Lipopolysaccharide in *Francisella tularensis* Subsp. *novicida*. *Biochemistry* **2006**, *45*, 14427−14440.

(9) Raetz, C. R.; Whitfield, C. Lipopolysaccharide Endotoxins. *Annu. Rev. Biochem.* **2002**, *71*, 635−700.

(10) Brandenburg, K.; Seydel, U. Investigation into the Fluidity of Lipopolysaccharide and Free Lipid A Membrane Systems by Fourier-Transform Infrared Spectroscopy and Differential Scanning Calorimetry. *Eur. J. Biochem.* **1990**, *191*, 229−236.

(11) Lins, R. D.; Straatsma, T. P. Computer Simulation of the Rough Lipopolysaccharide Membrane of *Pseudomonas aeroginosa*. *Biophys. J.* **2001**, *81*, 1037−1046.

(12) Soares, T. A.; Straatsma, T. P. Assessment of the Convergence of Molecular Dynamics Simulations of Lipopolysaccharide Membranes. *Mol. Simul.* **2008**, *34*, 295−307.

(13) Cornell, W.; Cieplak, P.; Bayly, C.; Gould, I.; Merz, K.; Ferguson, D.; Spellmeyer, D.; Fox, T.; Caldwell, J.; Kollman, P. A Second Generation Force Field for the Simulation of Proteins, Nucleic Acids and Organic Molecules. *J. Am. Chem. Soc.* **1995**, *177*, 5179−5197.

(14) Woods, R.; Dwek, A.; Edge, C. Molecular Mechanical and Molecular Simulations of Glycoproteins and Olilgosaccharides. 1. GLYCAM 93 Parameter Development. *J. Phys. Chem.* **1995**, *99*, 3832−3846.

(15) Brandenburg, K.; Seydel, U. Physical Aspects of Structure and Function of Membranes Made from Lipopolysaccharides and Free Lipid A. *Biochim. Biophys. Acta* **1984**, *775*, 225−238.

(16) Petrov, A. G.; Gawrisch, K.; Brezesinski, G.; Klose, G.; Möps, A. Optical Detection of Phase Transitions in Simple and Mixed Lipid-Water Phases. *Biochim. Biophys. Acta, Biomembr.* **1982**, *690*, 1−7.

(17) Piggot, T. J.; Holdbrook, D. A.; Khalid, S. Electroporation of the *E. coli* and *S. aureus* Membranes: Molecular Dynamics Simulations of

DOI: 10.1021/jp5119629
J. Phys. Chem. B 2015, 119, 5846−5856

Complex Bacterial Membranes. *J. Phys. Chem. B* **2011**, *115*, 13381−13388.
(18) Oostenbrink, C.; Villa, A.; Mark, A.; van Gunsteren, W. A Biomolecular Force Field Based on the Free Enthalpy of Hydration and Solvation: The GROMOS Force-Field Parameter Sets 53A5 and 53A6. *J. Comput. Chem.* **2004**, *25*, 1656−1676.
(19) Kukol, A. Lipid Models for United-Atom Molecular Dynamics Simulations of Proteins. *J. Chem. Theory Comput.* **2009**, *5*, 615−626.
(20) Kirschner, K.; Lins, R.; Maass, A.; Soares, T. A Glycam-Based Force Field for Simulations of Lipopolysaccharide Membranes: Parametrization and Validation. *J. Chem. Theory Comput.* **2012**, *8*, 4719−4731.
(21) Wu, E.; Engröm, O.; Jo, S.; Stuhlsatz, D.; Yeom, M.; Klauda, J. B.; Widmalm, G.; Im, W. Molecular Dynamics and NMR Spectroscopy Studies of *E. coli* Lipopolysaccharide Structure and Dynamics. *Biophys. J.* **2013**, *105*, 1444−1455.
(22) Snyder, S.; Kim, D.; McIntosh, T. Lipopolysaccharide Bilayer Structure: Effect of Chemotype, Core Mutations, Divalent Cations, and Temperature. *Biochemistry* **1999**, *38*, 10758−10767.
(23) Jorgensen, W.; Maxwell, D.; Tirado-Rives, J. Development and Testing of the OPLS All-Atom Force Field on Conformational Energetics and Properties of Organic Liquids. *J. Am. Chem. Soc.* **1996**, *118*, 11225−11236.
(24) *The PyMOL Molecular Graphics System*, version 1.4.1; Schrödinger, LLC: Cambridge, MA, 2011.
(25) Damm, W.; Frontera, A.; Tirado-Rives, J.; Jorgensen, W. L. OPLS All-Atom Force Field for Carbohydrates. *J. Comput. Chem.* **1997**, *18*, 1955−1970.
(26) Price, M. L. P.; Ostrovsky, D.; Jorgensen, W. L. Gas-Phase and Liquid-State Properties of Esters, Nitriles, and Nitro Compounds with the OPLS-AA Force Field. *J. Comput. Chem.* **2001**, *22*, 1340−1352.
(27) Kaminski, G.; Friesner, R.; Tirado-Rives, J.; Jorgensen, W. Evaluation and Reparametrization of the OPLS-AA Force Field for Proteins via Comparison with Accurate Quantum Chemical Calculations on Peptides. *J. Phys. Chem. B* **2001**, *105*, 6474−6487.
(28) Murzyn, K.; Bratek, M.; Pasenkiewicz-Gierula, M. Refined OPLS All-Atom Force Field Parameters for n-Pentadecane, Methyl Acetate, and Dimethyl Phosphate. *J. Phys. Chem. B* **2013**, *117*, 16388−16396.
(29) Stortz, C.; Johnson, G.; French, A.; Csonka, G. Comparison of Different Force Fields for the Study of Disaccharides. *Carbohydr. Res.* **2009**, *344*, 2217−2228.
(30) Jorgensen, W. L.; Chandrasekhar, J.; Madura, J. D.; Impey, R. W.; Klein, M. L. Comparison of Simple Potential Functions for Simulating Liquid Water. *J. Chem. Phys.* **1983**, *79*, 926−935.
(31) Aqvist, J. Ion-Water Interaction Potentials Derived from Free Energy Perturbation Simulations. *J. Phys. Chem.* **1990**, *94*, 8021−8024.
(32) Hess, B.; Kutzner, C.; van der Spoel, D.; Lindahl, E. GROMACS 4: Algorithms for Highly Efficient, Load-Balanced, and Scalable Molecular Simulation. *J. Chem. Theory Comput.* **2008**, *4*, 435−447.
(33) Hess, B.; Bekker, H.; Berendsen, H. J. C.; Fraaije, J. G. E. M. LINCS: A Linear Constraint Solver for Molecular Simulations. *J. Comput. Chem.* **1997**, *18*, 1463−1472.
(34) Miyamoto, S.; Kollman, P. A. SETTLE: An Analytical Version of the SHAKE and RATTLE Algorithms for Rigid Water Models. *J. Comput. Chem.* **1992**, *13*, 952−962.
(35) Essman, U.; Perela, L.; Berkowitz, M. L.; Darden, T.; Lee, H.; Pedersen, L. G. A Smooth Particle Mesh Ewald Method. *J. Chem. Phys.* **1995**, *103*, 8577−8592.
(36) Nose, S. A. Unified Formulation of the Constant Temperature Molecular-Dynamics Methods. *J. Chem. Phys.* **1984**, *81*, 511−519.
(37) Hoover, W. G. Canonical Dynamics: Equilibrium Phase-Space Distributions. *Phys. Rev. A* **1985**, *31*, 1695−1697.
(38) Parrinello, M.; Rahman, A. Polymorphic Transitions in Single Crystals: A New Molecular Dynamics Method. *J. Appl. Phys.* **1981**, *52*, 7182−7190.
(39) Szczelina, R.; Murzyn, K. DMG-α -A Computational Geometry Library for Multi-Molecular Systems. *J. Chem. Inf. Model.* **2014**, *54*, 3112−3123.
(40) Murzyn, K.; Róg, T.; Jezierski, G.; Takaoka, Y.; Pasenkiewicz-Gierula, M. Effects of Phospholipid Unsaturation on the Membrane/water Interface: A Molecular Simulation Study. *Biophys. J.* **2001**, *81*, 170−181.
(41) Jones, E., Oliphant, T., Peterson, P. *SciPy: Open Source Scientific Tools for Python*, 2001.
(42) Rao, V. *Conformation of Carbohydrates*; Harwood Academic Publishers: Amsterdam, The Netherlands, 1998, Chapter 4, pp 91−129.
(43) Nagle, J.; Tristram-Nagle, S. Structure of Lipid Bilayers. *Biochim. Biophys. Acta* **2000**, *1969*, 159−195.
(44) Kučerka, N.; Nieh, M.-P.; Katsaras, J. Fluid Phase Lipid Areas and Bilayer Thicknesses of Commonly Used Phosphatidylcholines As a Function of Temperature. *Biochim. Biophys. Acta, Biomembr.* **2011**, *1808*, 2761−2771.
(45) Murzyn, K.; Zhao, W.; Karttunen, M.; Kurdziel, M.; Róg, T. Dynamics of Water at Membrane Surfaces: Effect of Headgroup Structure. *Biointerphases* **2006**, *1*, 98−105.
(46) Georgi, B.; Costa, I.; Schliep, A. PyMix: the Python Mixture Package: A Tool for Clustering of Heterogeneous Biological Data. *BMC Bioinf.* **2010**, *11*, 9.
(47) Rohrer, D. C.; Sarko, A.; Bluhm, T.; Lee, Y. The Structure of Gentiobiose. *Acta Crystallogr.* **1980**, *B36*, 650−654.
(48) Cannon, J.; Raston, C.; Toia, R.; White, A. Crystal Structures of Z-O-β-D-Xylopyranosyl-(1→6)-β-D-Glucopyranosyloxy-*NNO*-Azoxymethane (macrozamin) and 5-*O*-Methyl-*myo*-Inositol (sequoyitol). *Aust. J. Chem.* **1980**, *33*, 2229−2236.
(49) Ihlenfeldt, W.; Bolton, E.; Bryant, S. The PubChem Chemical Structure Sketcher. *J. Cheminf.* **2009**, *1*, 20.
(50) Kim, H.; Park, B.; Kim, J.; Kim, S.; Lee, J.; Oh, S.; Enkhbayar, P.; Matsushima, N.; Lee, H.; Yoo, O.; et al. Crystal Structure of the TLR4-MD-2 Complex with Bound Endotoxin Antagonist Eritoran. *Cell* **2007**, *130*, 906−917.
(51) Ferguson, A.; Ködding, J.; Walker, G.; C, B.; Coulton, J.; Diederichs, K.; Braun, V.; Welte, W. Active Transport of an Antibiotic Rifamycin Derivative by the Outer-Membrane Protein FhuA. *Structure* **2001**, *9*, 707−716.
(52) Pandit, S.; Bostick, D.; Berkowitz, M. Mixed Bilayer Containing Dipalmitoylphosphatidylcholine and Dipalmitoylphosphatidylserine: Lipid Complexation, Ion Binding, and Electrostatics. *Biophys. J.* **2003**, *85*, 3120−3131.
(53) Cordomì, A.; Edholm, O.; Perez, J. Effect of Ions on a Dipalmitoyl Phosphatidylcholine Bilayer. a Molecular Dynamics Simulation Study. *J. Phys. Chem. B* **2008**, *112*, 1397−1408.
(54) Stepniewski, M.; Bunker, A.; Pasenkiewicz-Gierula, M.; Karttunen, M.; Róg, T. Effects of the Lipid Bilayer Phase State on the Water Membrane Interface. *J. Phys. Chem. B* **2010**, *114*, 11784−11792.

DOI: 10.1021/jp5119629
J. Phys. Chem. B 2015, 119, 5846−5856